Journal of Structural Geology, Vol. 15, No. 8, pp. 1007 to 1019, 1993
Printed in Great Britain

0191-8141/93 $06.00+0.00

Correlating mechanical data with microstructural observations in deformation experiments on synthetic two-phase aggregates

J. P. BLOOMFIELD* and S. J. COVEY-CRUMP

Rock Deformation Laboratory, Department of Geology, Manchester University, Oxford Road, Manchester M13 9PL, U.K.

(*Received* 13 *December* 1991; *accepted in revised form* 6 *October* 1992)

Abstract—A simple method of analysing the results of deformation experiments on synthetic two-phase aggregates is presented and applied to some tests on calcite–halite aggregates. The approach involves replacing the observed mechanical behaviour of real two-phase materials of coarse microstructure, with a phase volume fraction weighted mechanically equivalent representation in which each phase is assigned its own single-valued stress and its own single-valued strain. Such a representation can be solved for the stresses and strains in the two phases and the results compared with the stresses and strains as determined from the deformation microstructures. In principle, it is then possible to constrain which of the features of the microstructure are mechanically significant.

The stresses supported by the synthetic calcite–halite aggregates suggest a strong partitioning of the deformation into the halite at all volume fractions of calcite, and yet analysis of the halite strains from the deformation microstructures indicates that there is little or no strain partitioning between the phases. However, these conflicting results may be reconciled by using the calcite *contiguous* volume, rather than the actual calcite volume fraction, to characterize the strength of the aggregates with respect to those of their component phases.

INTRODUCTION

SEVERAL attempts to characterize the inelastic (but non-brittle) mechanical properties of a two-phase aggregate from the mechanical properties of its component phases, have been published in the recent geological literature. These have ranged from semi-theoretical discussions of the constraints on the problem (Tharp 1983, Jordan 1988, Handy 1990) to simulations of such deformation, both by experiment on synthetic aggregates (Price 1982, Jordan 1987, Ross *et al.* 1987) and by numerical modelling (Tullis *et al.* 1991, Wenk *et al.* 1991). In these studies the importance of microstructural features such as phase continuity have been emphasized along with phase volume fraction as controlling the relative contribution of each phase to the aggregate properties. However, in the absence of investigations into how microstructural features evolve with deformation, it remains unclear how they should be incorporated into aggregate flow laws.

In this study, an attempt is made to utilize the mechanical data provided by deformation experiments on synthetic two-phase aggregates to identify the mechanically significant features of the resulting microstructures. This is done by seeking to match the magnitude of the strains in the two phases as given by a simple phenomenological description of the observed mechanical behaviour of the aggregates, with the strains given by an analysis of the deformation microstructures themselves. The method is illustrated using the results of some experiments on synthetic calcite–halite aggregates.

*Present address: Aquifer Properties, British Geological Survey, Maclean Buildings, Crowmarsh Gifford, Wallingford, Oxfordshire OX10 8BB, U.K.

THE PHENOMENOLOGICAL DESCRIPTION

The following description of two-phase flow replaces the observed mechanical behaviour of real two-phase materials with a mechanically equivalent representation in which each phase is assigned its own single-valued stress and its own single-valued strain (subsequently referred to as the mechanically equivalent stresses and strains, respectively). These stresses and strains are the integrated total stresses and strains experienced by the respective phases in the aggregate. Accordingly, they are associated with the aggregate as a whole and cannot be ascribed to any individual grain within the polycrystal.

The description applies only where the mechanical properties of the aggregate can be expressed as some volume fraction weighted, linear combination of the mechanical properties of the component phases. This therefore excludes circumstances where a new phase, with mechanical properties different from the original components, arises during the deformation (e.g. by recrystallization or by some chemical interaction within the deforming system). More significantly, in materials deforming by intracrystalline slip processes, it requires that the heterogeneous nature of the two-phase flow be on a large scale in comparison with the scale of the inherently non-uniform deformation of crystal plasticity involving dislocations, i.e. that the work hardening behaviour of the two phases is not significantly influenced by strong interactions between the phases at the dislocation scale. If the grain size of one of the phases is sufficiently small, such interactions arise directly between the inclusion phase and the dislocations in the matrix phase. At larger grain sizes they occur between the statistically necessary and geometrically necessary

dislocations within each phase (respectively, dislocations which produce the deformation, and dislocations which merely solve strain incompatibility problems at the grain boundaries without contributing to the deformation, Ashby 1971). Since the significance of geometric dislocations increases with increasing grain boundary area, the phenomenological description of two-phase flow given here is restricted to aggregates in which the grain size of both phases is large (the coarse microstructure approximation). Apart from this intuitive argument there is no theoretical justification for the coarse microstructure approximation. However, it is widely employed in continuum models of two-phase deformation wherever the grain size of both phases is greater than a few microns (e.g. Chen & Argon 1979, Tullis *et al.* 1991), and has been shown experimentally to be valid in various metal alloys (Fischmeister & Karlsson 1977).

Geometric constraints on the description

Geometric constraints on the mechanically equivalent representation may be derived from the fundamental stereological relation

$$\phi_i = (L_i/L_t) = (A_i/A_t) = (V_i/V_t), \quad (1)$$

where (L_i/L_t) is the mean length fraction of the ith-phase on test lines through the aggregate, (A_i/A_t) is the mean areal fraction of the ith-phase on a section through the aggregate, and (V_i/V_t) is the volume fraction of the ith-phase in the aggregate (Underwood 1970). This relation holds independently of the orientation of the test lines or surfaces and also of the size, shape, orientation and distribution of the ith-phase, provided the measurements are obtained from statistically respresentative lines or sections or volumes.

By resolving the total force F_t into partial forces F_α and F_β acting on the α-phase and the β-phase, respectively,

$$\begin{aligned} F_t &= F_\alpha + F_\beta \\ &= F_\alpha(A_\alpha/A_\alpha) + F_\beta(A_\beta/A_\beta), \end{aligned} \quad (2)$$

where A_α and A_β are the respective phase areas. Dividing by the total area A_t and using equation (1), then

$$\sigma_t = \phi_\alpha\sigma_\alpha + \phi_\beta\sigma_\beta \quad (3)$$

in which σ_t is the stress acting on the aggregate, σ_α and σ_β are the mechanically equivalent stresses acting on the respective phases, and ϕ_α and ϕ_β are the volume fractions of those phases. By convention the α-phase is the weak phase.

Similarly, resolving the total shortening ΔL_t in terms of its components in the two phases,

$$\begin{aligned} \Delta L_t &= \Delta L_\alpha + \Delta L_\beta \\ &= \Delta L_\alpha(L_{\alpha 0}/L_{\alpha 0}) + \Delta L_\beta(L_{\beta 0}/L_{\beta 0}), \end{aligned} \quad (4)$$

where the subscript 0 refers to the initial length. Dividing by L_{t0} and using equation (1)

$$\varepsilon_t = \phi_\alpha\varepsilon_\alpha + \phi_\beta\varepsilon_\beta \quad (5)$$

in which ε_t is the engineering strain acting on the aggregate, and ε_α and ε_β are the mechanically equivalent engineering strains experienced by the respective phases. If necessary (depending on the type of mechanical data being described), strain-rates may be substituted for the strain terms in equation (5).

The generality of equation (1) means that equations (3) and (5) apply in all possible aggregate microstructures including the limiting cases of parallel and series arrangements of the constituents. Furthermore, by definition

$$1 = \phi_\alpha + \phi_\beta. \quad (6)$$

Constitutive constraints on the description

The constitutive relations for the component phases, in terms of their mechanically equivalent stresses and strains are rendered here as

$$\sigma_\alpha = \sigma_\alpha(\varepsilon_\alpha) \quad (7)$$

$$\sigma_\beta = \sigma_\beta(\varepsilon_\beta). \quad (8)$$

Using the coarse microstructure approximation these constitutive relations are the same as the flow laws for the single-phase end-members.

Applying the constraints

In uniaxial form, equations (3), (5), (6), (7) and (8) are five equations in eight variables. In any conceivable two-phase problem two variables are known or prescribed, typically ϕ_α (or ϕ_β) and ε_t (or σ_t), and so there are five equations in six unknowns. Hence the problem of fully characterizing the mechanical properties of two-phase aggregates of coarse microstructure, reduces to one of determining a sixth equation which contains no new variables, but which conveys new information, i.e. it is not merely a rearrangement of one of these equations and nor is it a relation involving only the two known variables. Suitable forms for this sixth equation include the constitutive relation $\sigma_t = \sigma_t(\varepsilon_t)$ as a function of ϕ_α, or the stress or strain partitioning between the two phases as a function ϕ_α. These equations can be determined empirically from suitably designed experiments, or can be theoretically prescribed with the aid of appropriate assumptions. Armed with the additional relation, the six equations may be solved simultaneously to yield the values of the six unknowns.

A graphical representation of the description

By rearranging and combining equations (3), (5) and (6) it may be shown that

$$(\sigma_\beta - \sigma_t)/(\varepsilon_t - \varepsilon_\beta) = (\sigma_t - \sigma_\alpha)/(\varepsilon_\alpha - \varepsilon_t) \quad (9)$$

(see the Appendix). Equation (9) implies that on a stress–strain graph the tie-line connecting $(\sigma_\alpha,\varepsilon_\alpha)$, $(\sigma_\beta,\varepsilon_\beta)$ and (σ_t,ε_t) is linear (Fig. 1). Hence, given the

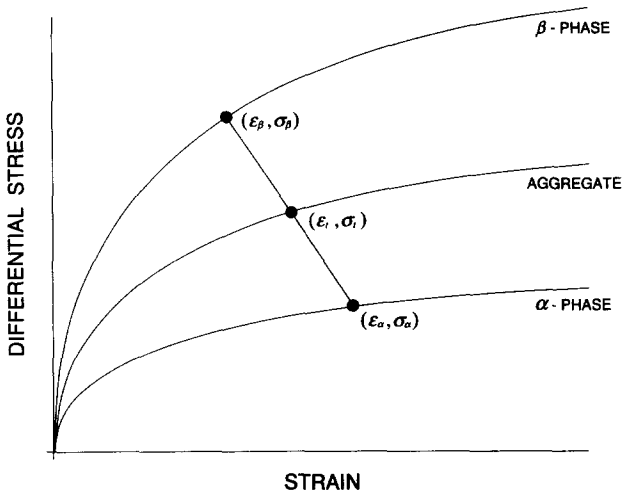

Fig. 1. A graphical representation of the phenomenological description, showing the linear tie-line connecting the stress–strain state of one phase with that of the other and with that of the aggregate.

stress–strain curves of the component phases and of the aggregate, together with any two (from different pairs) of the six stress and strain variables, all the other four variables can be determined. By using the deformation microstructures to evaluate the stress or strain in one of the phases, this observation has been exploited to determine the partitioning of deformation between the phases in a two-phase aggregate in a number of studies (e.g. Fischmeister & Karlsson 1977, Cho & Gurland 1988). Again it is emphasized that the use of the stress–strain curves of the component phases in this way is only valid under the coarse microstructure approximation.

The tie-line referred to above can never have a positive slope, for this would require the stronger phase to exhibit a larger strain than the weaker one, or the weaker phase to support a higher stress than the stronger one, both of which are precluded on energetic grounds (see Tullis *et al.* 1991 for further discussion).

EXPERIMENTAL TECHNIQUES AND METHODS OF ANALYSIS

Experimental procedure

Synthetic calcite–halite aggregates were prepared from Icelandic spar and analytical grade halite. Each phase was sieved, the halite from the 'as received' material and the calcite after grinding the Icelandic spar for a few seconds in an agate mill, to collect a grain size fraction of between 250 and 400 μm. The powders were then mixed in true volume proportions, inside the copper jackets (of 0.25 mm wall thickness) in which the specimens were contained during the deformation. Simple mechanical mixing with a spatula provided an adequate dispersion of the two phases through the aggregate (Fig. 2). The specimens were pressed in a double floating piston split-die at room temperature and at (nominally) 600 MPa. During the cold pressing a shape fabric developed in each of the two phases orthogonal to the die axis, indicating that the stress was not completely isostatic. Finally, the specimens were hot pressed for 5 h in the deformation apparatus, under true isostatic conditions at 200°C and 200 MPa confining pressure. The deformation experiments were conducted immediately following the completion of the 5 h period. The resulting starting material for each deformation experiment was a cylindrical specimen approximately 9.5 mm in diameter and 20 mm long. The halite recrystallized during hot pressing to produce equant grains with a lineal intercept size of about 300 μm, while the calcite remained poorly sintered and highly damaged, with a lineal intercept size of about 200 μm in the subsequent loading direction. The porosity remaining after hot pressing was a function of specimen composition; pure calcite samples had a porosity of about 13%, 0.6 volume fraction halite samples a porosity of about 6% and pure halite samples a porosity of about 1%. These porosities are slightly lower than those observed by Jordan (1987) in his synthetic calcite–halite aggregates.

The experiments were conducted in compression in a fluid (silicone oil) medium, triaxial (axisymmetric) deformation apparatus constructed, with some minor modifications, following a design by H. C. Heard (Rutter 1972). Specimens with halite volume fractions at 0.1 increments in the range 0 to 1, were deformed at a constant displacement-rate of 0.0495 mm min^{-1} (corresponding to a strain-rate of approximately $4 \times 10^{-5}\,s^{-1}$), 200 MPa confining pressure and 200°C. At least one experiment at each volume fraction was deformed to a strain of about 0.25 or more, while others were stopped at strains of 0.1, 0.2 and 0.3 for the microstructural analysis. The resulting stress–strain curves were reproducible (for specimens of given composition) to within ±4 MPa, emphasizing the consistent nature of the starting microstructure and the reliability of the specimen fabrication procedure.

Mechanical analysis

The aim of the mechanical analysis was to use the observed mechanical data to determine at any time during the deformation the mechanically equivalent stresses and strains σ_{cc}, ε_{cc}, σ_{hl}, ε_{hl} (where the subscript cc is used for calcite and hl for halite). To do this it was necessary first to find expressions for equations (7) and (8) and $\sigma_t = \sigma_t(\varepsilon_t, \phi_{hl})$. Since in each experiment the deformation history was approximately the same, a description of the determined stress–strain curves suffices. To this end, the strain–stress curves, i.e.

$$\varepsilon_{hl} = \varepsilon_{hl}(\sigma_{hl}) \tag{10}$$

$$\varepsilon_{cc} = \varepsilon_{cc}(\sigma_{cc}) \tag{11}$$

$$\varepsilon_t = \varepsilon_t(\sigma_t, \phi_{hl}) \tag{12}$$

were fitted with least-squares polynomials. Substituting equation (6) in equations (3) and (5), and equations (10) and (11) in equation (5) then

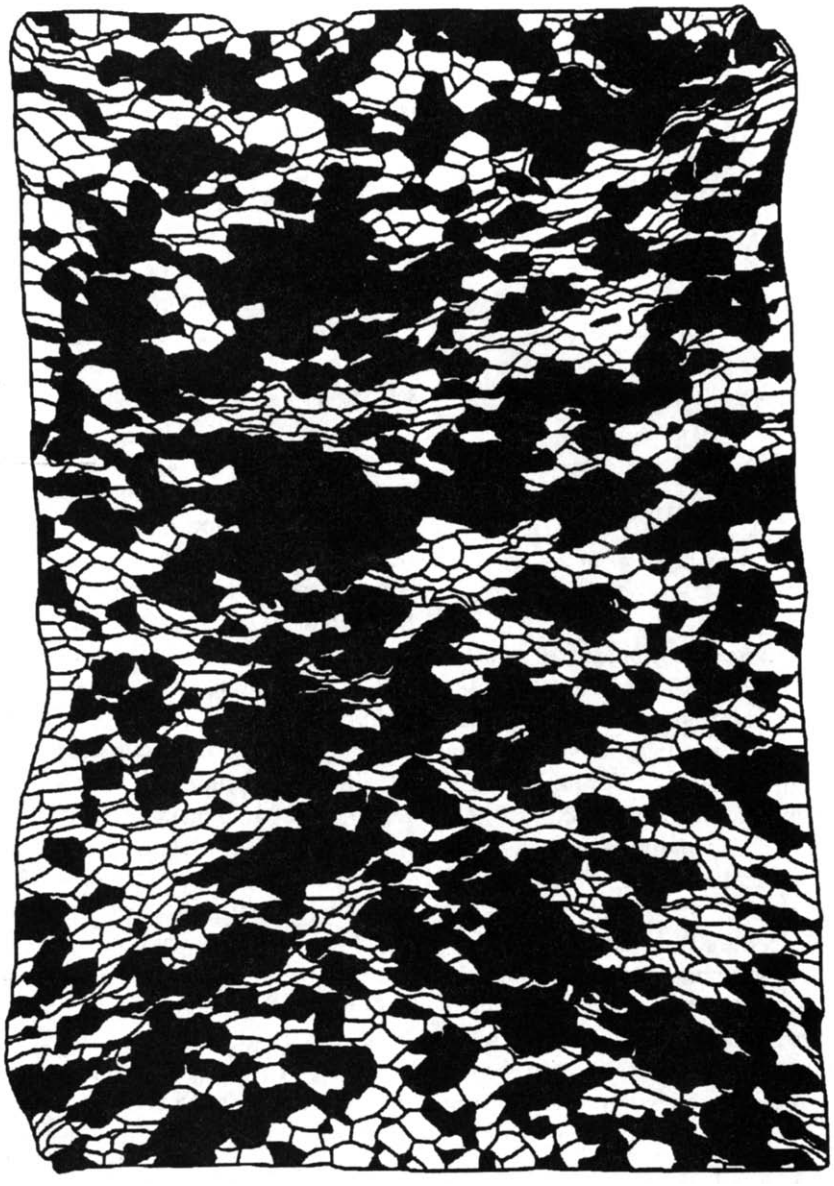

Fig. 2. A complete axial section through a sample containing 0.6 volume fraction calcite and deformed to a strain of 0.19. The areas of calcite are shown black and without any internal detail, while the indicated boundaries through the halite areas are the traced trails of calcite dust. The calcite dust trails indicate the deformation during cold pressing as well as during the deformation experiment. The development of conjugate shear zones emanating from the four corners of the sample can clearly be seen.

$$\sigma_t = \phi_{hl}\sigma_{hl} + (1 - \phi_{hl})\sigma_{cc} \quad (13)$$

$$\varepsilon_t = \phi_{hl}[\varepsilon_{hl}(\sigma_{hl})] + (1 - \phi_{hl})[\varepsilon_{cc}(\sigma_{cc})], \quad (14)$$

where halite is the α-phase and calcite the β-phase. Values of ε_t and ϕ_{hl} were chosen and equation (12) solved for σ_t. Equations (13) and (14) were then solved simultaneously to yield the two unknowns σ_{hl} and σ_{cc}, and then with these, equations (10) and (11) were solved for ε_{hl} and ε_{cc}. A combined bisection and Newton–Raphson routine was used to solve any non-linear equations.

Microstructural analysis

In order to evaluate the results of the mechanical analysis it is necessary to compare the values of the mechanically equivalent stresses and strains determined from that analysis with their values as determined independently from the deformation microstructures. Provided the coarse microstructure approximation is valid, then only one of σ_{cc}, ε_{cc}, σ_{hl} and ε_{hl} is required at given $(\varepsilon_t, \sigma_t)$ to constrain uniquely all the others (cf. Fig. 1). The aim of the microstructural analysis in this study was to determine the halite strain parallel to the bulk shortening direction using optical thin sections of samples deformed to various strains.

On inspection of the deformed microstructures it was discovered that during the mixing of the two powders the initial halite grains had been coated with a fine-grained ($<5\,\mu$m) calcite dust (generated during the milling of the Icelandic spar). This dust apparently had no influence on the behaviour of the halite, either during sintering or during deformation:

(a) the dust trails cross-cut the recrystallized halite

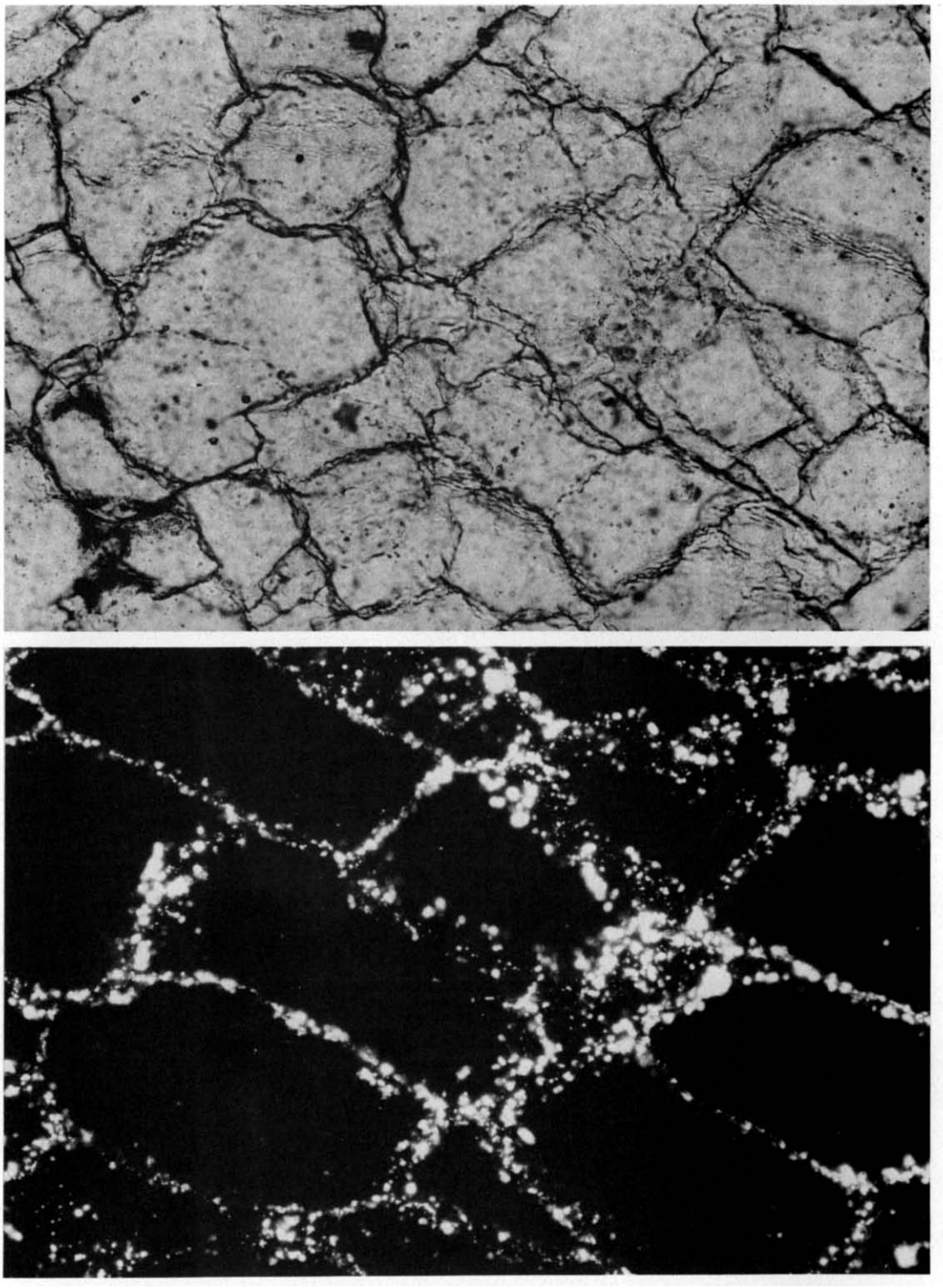

Fig. 3. Photomicrographs of a pure halite specimen doped with calcite dust (some of which is coarser than typical), which has been deformed to a strain of 0.16. The same field of view is visible in both micrographs. The recrystallized halite grain boundaries (visible in upper micrograph taken in plane polarized light) clearly cross-cut the calcite dust trails which outline the original halite particles (visible in the lower micrograph taken under cross polars). The base of each photomicrograph is 1.2 mm.

boundaries in arbitrary fashion (Fig. 3) implying that they had no influence on the recrystallization of the halite during sintering;

(b) there is no microstructural evidence that the dust either pinned, or was incorporated within, the recrystallized halite boundaries during deformation;

(c) experiments on pure halite specimens with a dust fraction added are mechanically indistinguishable from those without such a dust fraction.

Given these observations and the fact that the halite particles were initially (before cold pressing) equant, it was concluded that the dust trails could be used as passive markers for the strain experienced by the halite.

Longitudinal thin sections of the deformed aggregates were cut and the entire section photographed. The dust trails were traced from the photographs to produce an image approximately 15 × 30 cm, which was digitized by determining the x, y co-ordinates of a number of points around each grain perimeter. The area and moment of inertia tensor of each grain was determined by line integration around the points characterizing its boundary (using the routine of Tough & Miles 1984, Tough 1988), and the grain was thereby specified in orientation by the orientation of the principal axes of the inertia tensor, and in shape (aspect ratio) by the square root ratio of the principal values of that tensor.

For each grain the component of strain ε_i (where i is used as a grain label) parallel to the specimen axis, is given by

$$(1 + \varepsilon_i) = \{R_i^{1/3}[(\cos^2\theta_i/R_i) + R_i\sin^2\theta_i]\}^{-1/2}, \quad (15)$$

where R_i is the aspect ratio of the grain, θ_i is the angle between the specimen axis and the long axis of the grain, and constant volume, axisymmetric deformation from initially equant grains has been assumed (see the Appendix). For perfectly axisymmetric deformation $\theta = 90°$ and $\varepsilon_i = \varepsilon_3$. However, local strain gradients due to the impingement of the halite grains into the stronger calcite grains and to specimen end effects, result in the deviation of θ from 90° particularly at large ($\varepsilon_t > 0.2$) strains (Fig. 2). The use of equation (15) is therefore under the assumptions that each grain deforms axisymmetrically and that this axis lies in the plane of the section. Any departure from the latter assumption will lead to an underestimate of strain, for the principal strain axes then no longer lie in the section plane. However, given that the entire section was analysed, that for the specimen as a whole $\sigma_2 = \sigma_3$, and that the shape orientations of the grains are disposed symmetrically about the specimen axis (i.e. axisymmetry was maintained for the whole sample, cf. Fig. 2), it was anticipated (and confirmed by the strain analyses on pure halite specimens, see below) that these errors are small.

Given ε_i for each grain, the total halite strain parallel to the specimen compression direction $(\varepsilon_{hl})_{ob}$ is

$$(\varepsilon_{hl})_{ob} = \sum_i (A_i/A_t)\varepsilon_i, \quad (16)$$

where the summation is carried out over the entire number of grains in the section, A_i is the area of the ith grain, and A_t is the total area of halite. This expression is derived in the same way as equation (5) but with the use of the stereological observation that the length fraction of the ith-phase on test lines (here parallel with the bulk compression direction and thereby indicating the axial strain) across a section through an aggregate, is equal to the areal fraction of the phase on that section (equation 1).

The strain imposed during the cold pressing was determined in this way, as a function of composition, from hot pressed but undeformed specimens of 0.2, 0.4, 0.6, 0.8 and 1 volume fraction halite. This strain was subtracted from that given by equation (16) for the deformed specimens, to give the strain imposed during the deformation.

By identifying the mechanically equivalent halite strain with the grain-size weighted sum of the strains experienced by each halite grain in the aggregate, it is implicitly assumed that the deformation of the aggregate is statistically homogeneous at the grain scale (or rather, given the use of the end-member flow laws in the rest of the analysis, is at least as statistically homogeneous at the grain scale as it is in the single-phase polycrystal). This assumption (the quasi-homogeneous continuum approximation, Gurland 1979) is justified on the basis that the strain heterogeneities observed across the deformation microstructures are a much stronger function of aggregate strain than of aggregate composition. It is necessary because the individual grains are the smallest unit of the microstructure which can be identified in the optical microstructures.

RESULTS

Experimental

The stress–strain curves obtained from the experiments are shown in Fig. 4. For each volume fraction, the stress–strain curve shown falls near the middle of the

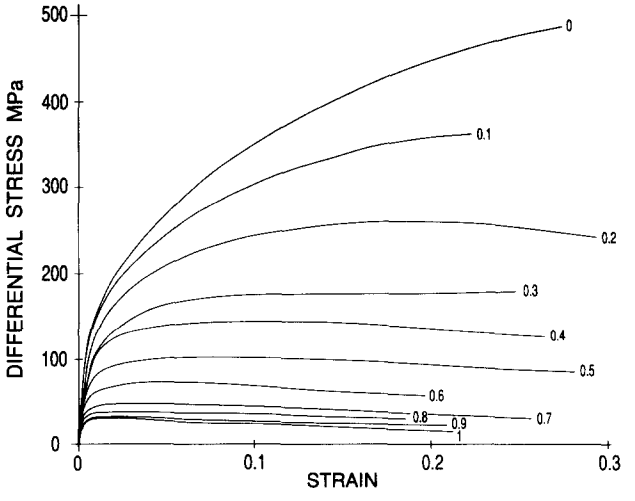

Fig. 4. Calcite–halite stress–strain curves produced at the indicated volume fraction halite.

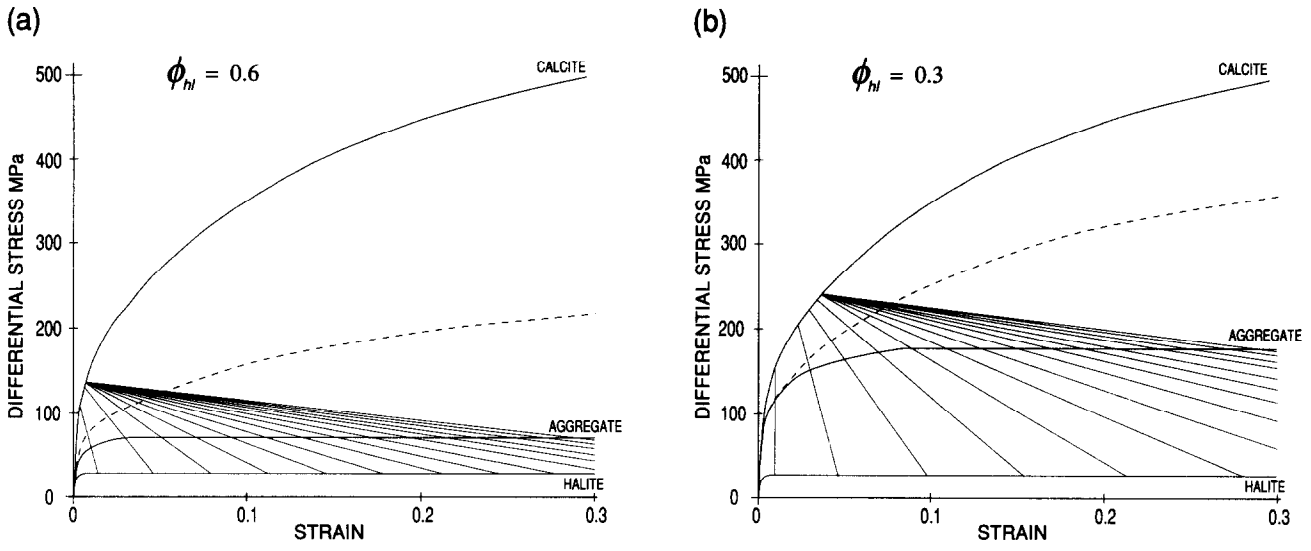

Fig. 5. Calculations of the tie-lines connecting the stress–strain states of the calcite and halite at (a) 0.6 volume fraction halite and (b) at 0.3 volume fraction halite. The dashed curves indicate the predicted aggregate stress–strain curves under the prescription that the halite strain equals that of the calcite.

range of reproducibility results obtained at that composition. The stress data are corrected for the load supported by the copper jacketing material and, assuming constant volume, homogeneous deformation, for the cross-sectional area change of the specimen during the deformation. Microstructural examination indicated that at all volume fractions the halite deformed by intracrystalline slip processes, while the calcite deformed partly by intracrystalline slip–mechanical twinning and partly by cataclasis.

The stresses supported by the aggregates as a function of both aggregate strain and volume fraction halite, are similar to those found by Jordan in his synthetic calcite–halite experiments conducted under the same conditions (Jordan 1988). As Jordan observed, even small additions of halite produce a large reduction in strength of the aggregate when compared with the strength of the pure calcite specimens. In all tests with halite volume fractions of greater than 0.2, the stress–strain curves become flat-topped and in several an apparent work softening is observed. The significance of the work softening is uncertain, for in repeat tests conducted on larger (25 mm diameter and 50 mm long) pure halite specimens, it was not observed. Consequently in the analyses which follow, the maximum stress of the stress–strain curve is used for all strains where apparent work softening was observed, although it is recognized that the softening may be real.

Mechanical analysis

Figure 5 shows the results of the mechanical analysis of the stress–strain curves for aggregates with halite volume fractions of 0.6 and 0.3. Tie-lines indicate the calculated mechanically equivalent stresses and strains in each phase as a function of aggregate strain. Also shown in the figure are the predicted stress–strain curves of the aggregate for each of the two volume fractions in the iso-strain case (i.e. assuming that $\varepsilon_{hl} = \varepsilon_{cc} = \varepsilon_t$), as given by incrementing the value of ε_t and solving for the requisite stresses in equations (10), (11) and (13). It is observed that at all volume fractions the aggregate stress–strain curve is significantly weaker than that predicted if the strains in the two phases are equal, i.e. the strain is apparently partitioned into the halite. This partitioning increases with increasing volume fraction halite and aggregate strain (Fig. 6). If the aggregate stress–strain curve becomes flat-topped the calcite apparently stops deforming and behaves as a rigid stressed inclusion (an inevitable consequence of equation 3 given that in such circumstances the mechanically equivalent calcite stress must increase to accomplish further deformation for it is work hardening, and yet the other two stresses are constant).

Microstructural analysis

Comparison of the strains calculated from the pure halite microstructures with the actual strains experienced by those aggregates, shows that equation (16) leads to the expected (see discussion of equation 15) small underestimate of the axial strain (Fig. 7). This underestimate is of the order of a strain of 0.01, although at larger strains ($\varepsilon_t > 0.25$) the discrepancy becomes larger. It is assumed that these underestimates are no larger in the two-phase aggregates than they are in the pure halite samples for the same reason as was used to justify the quasi-homogeneous continuum approximation, i.e. that the effect of increasing aggregate strain on the strain heterogeneities across the samples is much greater than the effect of increasing volume fraction calcite at given strain. The three points for the sample deformed to a strain of approximately 0.2 were obtained from independent tracings of the same photomosaic (by the authors and K. H. Brodie), and show that the strain underestimate is essentially independent of observer bias in interpretating the strain marker morphology.

Table 1 compares the halite strains determined from

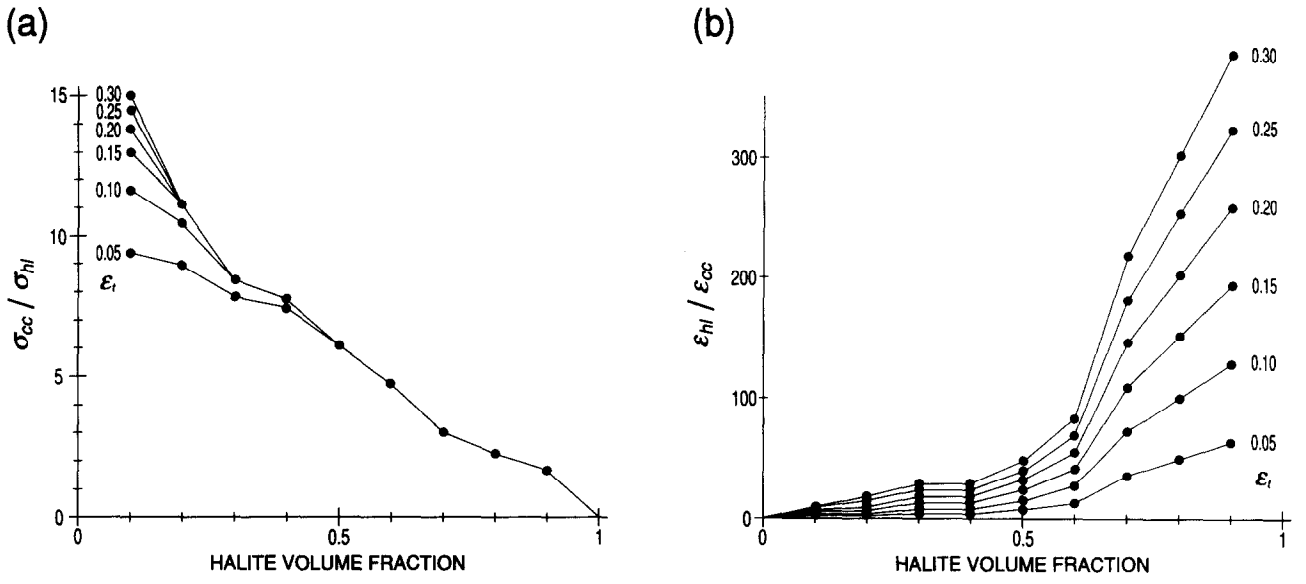

Fig. 6. The partitioning, as calculated from the stress–strain curves of Fig. 4, of (a) the stress and (b) the strain between the two phases as a function of halite volume fraction and aggregate strain.

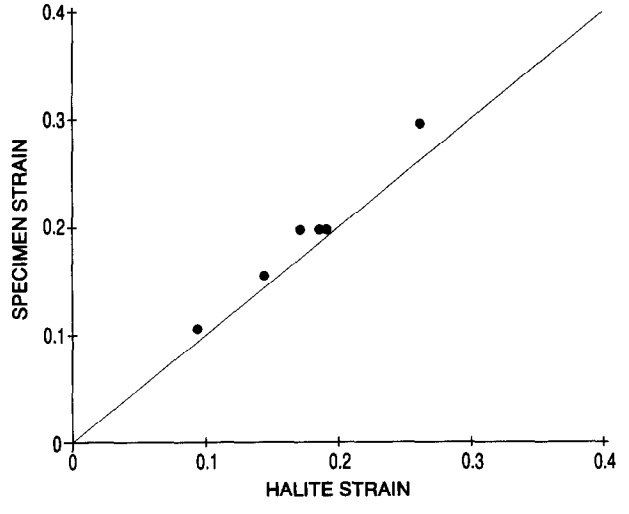

Fig. 7. A comparison of the bulk specimen axial strain with the observed halite strain as given by equation (16) (correcting for the strain induced during cold pressing), for pure halite experiments. The indicated line is that for perfect correspondence between the two.

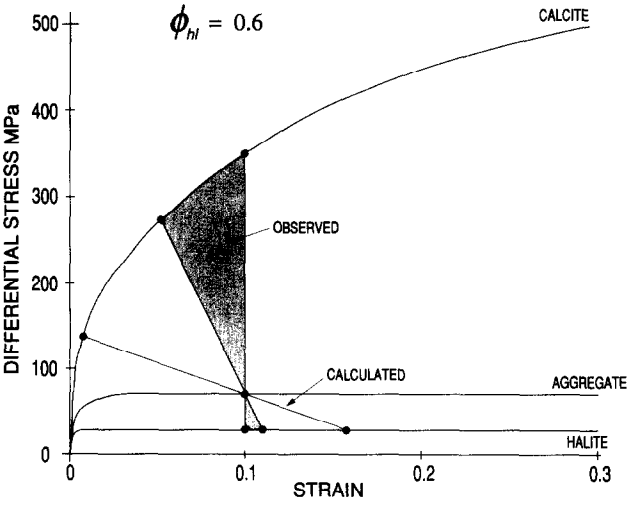

Fig. 8. Comparison of the tie-lines connecting the stress–strain states of the calcite and halite at an aggregate strain of 0.1 and 0.6 volume fraction halite, where the calculated tie-line is that given by the mechanical analysis, and the observed field of tie-lines is that prescribed by the halite strains determined from the deformation microstructures. The bounds on the observed field are for the halite strain as given by equation (16) on the assumption that the equation is accurate (iso-strain bound), and on the assumption that it leads to a strain underestimate of 0.01 (sloping bound).

Table 1. Data from the five analysed deformation microstructures, comparing the halite strain predicted from the mechanical analysis ε_{hl}, with that observed $(\varepsilon_{hl})_{ob}$; and comparing the apparent calcite volume fraction, $(\phi_{cc})_{app}$, with the calcite contiguous volume, V_{cc}. The error given for the contiguous volume of calcite corresponds to an error of ±20 μm on the calcite intercept size in the direction of loading

ϕ_{cc}	ε_{agg}	ε_{hl}	$(\varepsilon_{hl})_{ob}$	$(\phi_{cc})_{app}$	V_{cc}
0.8	0.09	0.20	0.11	0.73	0.67 ± 0.01
0.8	0.16	0.49	0.21	0.62	0.64 ± 0.01
0.4	0.10	0.16	0.10	0.13	0.15 ± 0.02
0.4	0.19	0.31	0.18	0.11	0.14 ± 0.02
0.2	0.18	0.22	0.18	0.02	0.02 ± 0.02

the microstructures using equation (16) with those determined from the analysis of the stress–strain curves (i.e. the mechanically equivalent halite strain). For a halite volume fraction of 0.2 there is a small partitioning of strain into the halite phase which is much less than predicted by the mechanical analysis, while for the other volume fractions the halite strain equals the aggregate strain i.e. there is no strain partitioning. The errors indicated in Fig. 7 for the halite strain obtained from the microstructures do not substantially alter this conclusion. This is shown by Fig. 8, in which the tie-lines obtained using values of halite strain which are 1% strain larger than the aggregate strain, are still much steeper than those obtained by the mechanical

analysis for the same halite volume fraction. Given the observed stress–strain curves, the geometry of the tie-line construction indicates that the significance of the errors incurred by the use of equation (16) diminishes with increasing aggregate strain and increasing halite volume fraction.

DISCUSSION

The observation from the calcite–halite microstructures that there is little or no strain partitioning between the two phases during deformation, conflicts with the observation from the analysis of the mechanical results that the aggregate stress–strain curves are much weaker than predicted for the iso-strain case. In deriving the constraint equations for the mechanically equivalent representation two assumptions were made:

(a) that the aggregate properties are some weighted, linear combination of the properties of the component phases (the coarse microstructure approximation); and

(b) that the weighting factor is the volume fraction of the respective phases.

The first assumption is considered to be valid given that the calcite–halite microstructures are extremely coarse. Hence it follows that the cause of the conflicting results resides in the use of volume fraction as the weighting factor, i.e. in the inadequacy of the geometric constraint equations to provide real constraints on the deformation behaviour. To determine the appropriate weighting factor, the derivation of the geometric constraint equations was dropped, and the mechanical analysis was rewritten to solve for the apparent volume fractions $(\phi_\alpha)_{app}$ and $(\phi_\beta)_{app}$ given a strain partitioning function. The deformation microstructures could then be re-examined to determine what, if any, feature corresponded with the apparent volume fractions.

Solving for apparent volume fractions

Using apparent volume fractions equations (3) and (5) are

$$\sigma_t = (\phi_\alpha)_{app}\sigma_\alpha + (\phi_\beta)_{app}\sigma_\beta \quad (17)$$

$$\varepsilon_t = (\phi_\alpha)_{app}\varepsilon_\alpha + (\phi_\beta)_{app}\varepsilon_\beta \quad (18)$$

with additionally

$$1 = (\phi_\alpha)_{app} + (\phi_\beta)_{app} \quad (19)$$

$$\varepsilon_\alpha = \varepsilon_\alpha(\varepsilon_t, \phi_\alpha), \quad (20)$$

where equation (20) expresses the strain partitioning as a function of aggregate strain and the true volume fraction ϕ_α. It is observed that since equations (17), (18) and (19) are of the same form as equations (3), (5) and (6), the linear tie-line property (equation 9) is still valid. Equations (10), (11) and (12) are retained (as is equation 6 so that the two new apparent volume fraction variables are accommodated in the system by the two new equations 19 and 20). Combining the new equations, equations (13) and (14) become in the α/β notation

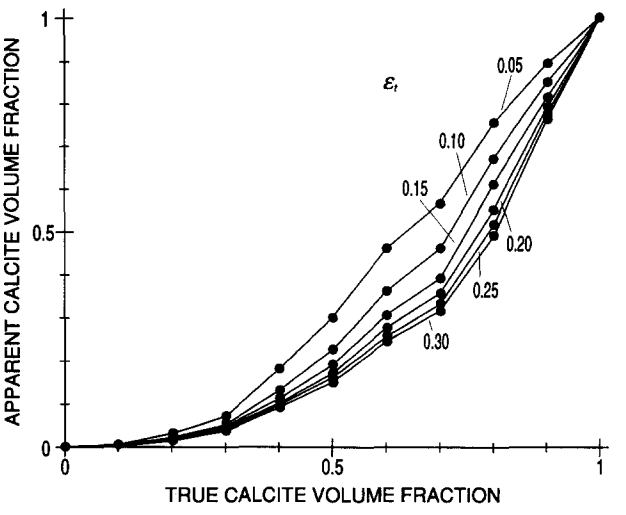

Fig. 9. The apparent calcite volume fraction as determined from the mechanical data presented in Fig. 4 under the iso-strain assumption, and plotted as a function of true calcite volume fraction for the indicated aggregate strains.

$$\sigma_t = [1 - (\phi_\beta)_{app}]\sigma_\alpha + (\phi_\beta)_{app}\sigma_\beta \quad (21)$$

$$\varepsilon_t = [1 - (\phi_\beta)_{app}][\varepsilon_\alpha(\sigma_\alpha)] + (\phi_\beta)_{app}[\varepsilon_\beta(\sigma_\beta)]. \quad (22)$$

Prescribing ϕ_α and ε_t, then ε_α is given by equation (20) and σ_α and σ_t may be found from equations (10) and (12). Hence rearranging equation (22) for σ_β and substituting in equation (21), $(\phi_\beta)_{app}$ may be found.

This procedure is simplified in the present case if the small strain partitioning observed at 0.2 volume fraction halite is ignored so that at all ϕ_{hl} then $\varepsilon_{hl} = \varepsilon_{cc} = \varepsilon_t$. Equations (10), (11) and (12) may then be used to find σ_{hl}, σ_{cc} and σ_t and these may be substituted directly into equation (21) to give

$$(\phi_{cc})_{app} = (\sigma_t - \sigma_{hl})/(\sigma_{cc} - \sigma_{hl}). \quad (23)$$

Figure 9 shows the apparent calcite volume fractions calculated from equation (23) as a function of true calcite volume fraction at various aggregate strains, given the stress–strain curves of Fig. 4. As may be expected from the fact that the aggregate stresses are weaker than predicted, the aggregates behave as though they contain considerably less calcite than is actually the case.

Re-examination of the deformation microstructures

The problem now becomes one of determining what, if any, feature of the deformation microstructure correlates with the apparent calcite volume fraction. The geometric constraint equations (3) and (5) take no account of the distribution of the phases through the aggregate. Hence the component stresses and strains are defined as if all the grains are arranged in an end-loaded, single-phase polycrystal. In real microstructures however, the phases are in general, discontinuously distributed. The stresses in the strong phase therefore reflect not pure end-loading, but rather an 'end-load' component equal to the stress in the weak phase, plus a

component which is due to the transfer of load from the weak to strong phase through the shear stresses generated by the difference in deformation-rates across their shared boundaries. Hence it may be expected that the geometric constraint equations will contain some microstructural variable which accounts specifically for the area of boundary shared between the two phases. Contiguity provides such a variable, and for this reason a contiguity analysis was conducted on the five specimens analysed previously for the halite strain.

Contiguity C is defined as the fraction of the total internal surface area of a phase that is shared by particles of the same phase

$$C_\beta = 2S_{\beta\beta}/(2S_{\beta\beta} + S_{\alpha\beta}), \tag{24}$$

where $S_{\beta\beta}$ is the shared boundary area between β-grains and $S_{\alpha\beta}$ is the area of interphase boundary, both per unit volume (Gurland 1958). By being a surface area dependent term, contiguity may be determined from intercept counting on a planar section through an aggregate. This follows from the often derived relationship

$$S_{\beta\beta} = 2P_{\beta\beta}, \tag{25}$$

where $P_{\beta\beta}$ is the number of intercepts made by shared $\beta\beta$ boundaries per unit length of test line (e.g. Underwood 1970, pp. 31–32). Using equation (25), equation (24) becomes

$$C_\beta = 4P_{\beta\beta}/(4P_{\beta\beta} + 2P_{\alpha\beta}). \tag{26}$$

It may further be shown that a contiguous volume V_β is given by

$$V_\beta = C_\beta\phi_\beta \tag{27}$$

(Gurland 1979). From the definition of contiguity, it follows that a given grain is not either in the contiguous volume or not. Rather each individual grain makes a grain size weighted contribution to the contiguous volume of its phase according to the proportion of its surface area that it shares with other grains of like phase.

In an aggregate in which the phases are discontinuously distributed it is the contiguous volume of the strong phase which is of significance for it is this which determines the extent to which the load transfer from weak to strong can occur (i.e. the potential for load transfer increases as strong phase contiguity decreases). In the calcite–halite analysis it is therefore the contiguous volume of calcite which needs to be determined. Unfortunately equation (26) could not be used because the calcite grains were so heavily damaged by the specimen preparation and deformation that it was not possible to make reliable tracings of calcite–calcite grain boundaries from photographs of the microstructures. However, the calcite grain boundaries were clearly visible under the microscope, and so to take advantage of this, the equation defining the contiguity of a phase was re-expressed in terms of the average lineal intercept length d_β of the phase (determinable under the microscope), the volume fraction of the phase, and the counts of the interphase boundaries (determinable from the tracings). Then

$$C_\beta = 1 - (d_\beta P_{\alpha\beta}/2\phi_\beta) \tag{28}$$

(see the Appendix). Counts of calcite–halite boundaries were made from the traced images of the microstructures using linear test lines which were parallel to the specimen axis, and regularly spaced across the full width of the specimen. Between 400 and 1000 interphase boundaries were sampled (depending on the volume fraction of halite) on each tracing. The mean intercept size of the calcite in the same direction was estimated directly under the microscope, by counting intercepts and applying the relation

$$d_\beta = 2\phi_\beta/(2P_{\beta\beta} + P_{\alpha\beta}) \tag{29}$$

(see the Appendix). These counts were carried out on two samples which had undergone a total strain of 0.2 and which had 0.8 and 1 volume fraction calcite, respectively. The intercept size determined was corrected for axial strain for use in the other microstructures. The error introduced here includes primarily the variability in the initial calcite grain size between specimens and the assumption that the calcite strain is accommodated entirely by a grain shape change. Both these factors must be rather less than the $\pm 20\ \mu$m error introduced by the difficulty in determining exactly what was and what was not a calcite grain boundary even when viewed under the microscope.

The calcite contiguous volumes determined from equations (28) and (27) are compared with $(\phi_{cc})_{app}$ in Table 1 where the apparent calcite volume fraction has been determined from equations (21) and (22) for the 0.2 halite volume fraction specimens (i.e. the observed strain partitioning is accounted for), and from equation (23) for the other specimens. There is good agreement between the two within the errors involved.

Interpretative comments

The preceding analysis suggests that the mechanical behaviour of the calcite–halite aggregates described here may be accounted for by the following system of equations

$$\sigma_t = C_{cc}\phi_{cc}\sigma_{cc} + (1 - C_{cc}\phi_{cc})\sigma_{hl} \tag{30}$$

$$\varepsilon_t = C_{cc}\phi_{cc}\varepsilon_{cc} + (1 - C_{cc}\phi_{cc})\varepsilon_{hl} \tag{31}$$

$$\sigma_{cc} = \sigma_{cc}(\varepsilon_{cc}) \tag{32}$$

$$\sigma_{hl} = \sigma_{hl}(\varepsilon_{hl}) \tag{33}$$

which are four equations in eight variables. All the grains of a phase are used to determine the stresses and strains of that phase, and the calcite contiguity, which accounts for the microstructure of the aggregate, is determined over the same domain as used to determine those stresses and strains (in this case the whole specimen). This conclusion is dependent on the validity of the coarse microstructure approximation, which could in principle (though in these specimens, not in practice), be verified by determining σ_{cc} or ε_{cc} to confirm that the linear tie-line property (equation 9) holds.

Equations (30) and (31) require theoretical justifi-

cation. Shear-lag theories seem to offer the best prospect for achieving this (cf. Gurland 1979) but no attempt to apply them is made here. However, some qualitative comments are offered.

In the case that all the grains of the strong phase are arranged in a continuous framework in the loading direction, the strong phase contiguity is unity, and equations (30) and (31) reduce to the original constraint equations (3) and (5). In such circumstances the two-phase flow problem may be treated using the notion of a load-bearing framework (Tharp 1983). Since phase contiguity is directly and unequivocally related to phase continuity only at its limits of 0 and 1, this is the only instance in which equations (30) and (31) can be treated in this way. To consider the aggregate stress as composed of a part arising from the strong phase grains in the framework and a part arising from the rest of the aggregate (isolated strong phase and weak phase grains) requires that the isolated strong phase grains be distinguished in microstructural analyses because they do not experience the same strain as the weak phase (i.e. the problem becomes a three-phase one). Moreover, the notion of a load-bearing framework may be of limited utility because as observed previously (e.g. Handy 1990) and confirmed here (Fig. 9, given the contiguity interpretation), such frameworks seem to break down ($C_\beta < 1$) at very small strains–volume fraction weak phase.

In the case that all the grains of the strong phase are fully dispersed, the strong phase contiguity is zero and the aggregate stress and strain are those of the weak phase. In such circumstances the two-phase flow problem becomes that of the flow of a viscous fluid containing rigid particles (e.g. Soo 1991).

In all intermediate cases ($0 < C_\beta < 1$), contiguity analyses can provide a useful contribution to the problem of two-phase flow in a manner in which the load-bearing framework and viscous fluid approaches do not permit. In the calcite–halite aggregates reported here the load transfer from the halite to the calcite results in a calcite stress which is greater than anticipated in the absence of microstructural considerations. Consequently, the calcite experiences a larger strain, and the strain required of the halite is decreased. Figure 9 implies that as the deformation proceeds the calcite contiguity decreases, thereby permitting more load transfer and hence allowing the approximately iso-strain condition to be maintained. This microstructural evolution continues even when the aggregate is nominally deforming at steady-state, i.e. when the aggregate stress–strain curve is flat-topped. However, the fact that the curves of constant strain in Fig. 9 become closer together as the strain increases, suggests that there is a limit to this process which is a function of the volume proportions of the two phases. Beyond this limit other processes not accommodated in this analysis (e.g. dynamic recrystallization or diffusive mass transfer processes) are required if the microstructure is to evolve further.

In conclusion, it seems that provided equations (30) and (31) are found to have general and theoretical validity, then contiguity analyses present a relatively simple means of tracing the evolution of aggregate mechanical properties as the relative strength of the two phases changes (perhaps through changes in the deformation environment) and as the deformation microstructure develops.

CONCLUSIONS

(1) A method is presented for determining the stresses and strains experienced by the components of a two-phase aggregate of coarse microstructure using the stress–strain curves of the aggregate and the single-phase end-members. It is used to determine the strain experienced by the halite in some synthetic calcite–halite aggregates, both as a function of aggregate strain and as a function of calcite volume fraction. In all cases the aggregate stress–strain curves suggest a strong partitioning of the deformation into the halite.

(2) The strain experienced by the halite is determined independently from an analysis of the deformation microstructures of the synthetic aggregates. In all cases there appears to be very little partitioning of the deformation into the halite, i.e. the halite strain is approximately the same as that of the aggregate.

(3) The conflicting values of halite strain given by the two methods may be reconciled if instead of the phase volume fractions, the contiguous volume of the calcite is used to weight the contribution of each phase to the aggregate properties.

(4) The analysis provides a method for using mechanical and microstructural data simultaneously to constrain the bulk flow properties of two-phase aggregates. It also highlights the need for contiguity analyses on deformation microstructures, particularly with a view to determining how the contiguity of the strong phase evolves during deformation.

Acknowledgements—This work was begun whilst one of us (J. P. Bloomfield) was holding a NERC research studentship (GT4/87/GS/63) at Imperial College of Science, Technology and Medicine, London, and was completed at Manchester University while we were both holding research assistantships (J. P. Bloomfield funded by Manchester University and S. J. Covey-Crump funded on NERC research grant GR3/6174). Discussions with Mark Handy provided the inspiration for several of the ideas presented here, and we have also benefited from discussions with Ernie Rutter and Katie Brodie. We acknowledge the important contribution made by Rob Holloway in his upgrading and maintenance of the deformation apparatus used for our experiments. The text benefited substantially from review by T. E. Tullis and R. J. Twiss.

REFERENCES

Ashby, M. F. 1971. The deformation of plastically non-homogeneous alloys. In: *Strengthening Methods in Crystals* (edited by Kelly, A. & Nicholson, R. B.). Applied Science Publishers, London, 137–192.

Chen, I. W. & Argon, A. S. 1979. Steady state power law creep in heterogeneous alloys with coarse microstructures. *Acta metall.* **27**, 785–791.

Cho, K. & Gurland, J. 1988. The law of mixtures applied to the plastic deformation of two-phase alloys of coarse microstructures. *Metall. Trans.* **19A**, 2027–2040.

Fischmeister, H. & Karlsson, B. 1977. Plasticity of two-phase materials with a coarse microstructure. *Z. Metallk.* **68,** 311–327. (In German.)
Gurland, J. 1958. The measurement of grain contiguity in two-phase alloys. *Trans. A.I.M.E.* **212,** 452—455.
Gurland, J. 1979. A structural approach to the yield strength of two-phase alloys with coarse microstructures. *Mater. Sci. Engng* **40,** 59–71.
Handy, M. R. 1990. The solid-state flow of polymineralic rocks. *J. geophys. Res.* **95,** 8647–8661. (Corrected version. *J. geophys. Res.* **97,** 1897–1899.)
Jordan, P. G. 1987. The deformational behaviour of bimineralic limestone–halite aggregates. *Tectonophysics* **135,** 185–197.
Jordan, P. G. 1988. The rheology of polymineralic rocks—an approach. *Geol. Rdsch.* **77,** 285–294.
Price, R. H. 1982. Effects of anhydrite and pressure on the mechanical behaviour of synthetic rocksalt. *Geophys. Res. Lett.* **9,** 1029–1032.
Ramsay, J. G. 1967. *Folding and Fracturing of Rocks.* McGraw-Hill, New York.
Ross, J. V., Bauer, S. J. & Hansen, F. D. 1987. Textural evolution of synthetic anhydrite-halite mylonites. *Tectonophysics* **140,** 307–326.
Rutter, E. H. 1972. The influence of interstitial water on the rheological behaviour of calcite rocks. *Tectonophysics* **14,** 13–33.
Soo, S. L. 1991. Comparisons of formulations of multiphase flow. *Powder Technol.* **66,** 1–7.
Tharp, T. M. 1983. Analogies between the high temperature deformation of polyphase rocks and the mechanical behaviour of porous powder metal. *Tectonophysics* **96,** T1–T11.
Tough, J. G. 1988. The computation of the area, centroid, and principal axes of a polygon. *Comput. & Geosci.* **14,** 715–717.
Tough, J. G. & Miles, R. G. 1984. A method for characterizing polygons in terms of the principal axes. *Comput. & Geosci.* **10,** 347–350.
Tullis, T. E., Horowitz, F. G. & Tullis, J. 1991. Flow laws of polyphase aggregates from end member flow laws. *J. geophys. Res.* **96,** 8081–8096.
Underwood, E. E. 1970. *Quantitative Stereology.* Addison-Wesley, Reading, Massachusetts.
Wenk, H.-R., Bennett, K., Canova, G. R. & Molinari, A. 1991. Modelling plastic deformation of peridotite with the self-consistent theory. *J. geophys. Res.* **96,** 8337–8349.

APPENDIX

Derivation of the tie-line equation (9)

Rearranging equation (3) and subtracting σ_t from both sides

$$(\sigma_\beta - \sigma_t) = (\sigma_t - \phi_\beta\sigma_t - \phi_\alpha\sigma_\alpha)/\phi_\beta.$$

Substituting equation (6) and rearranging

$$(\sigma_\beta - \sigma_t) = (\sigma_t - \sigma_\alpha)(1 - \phi_\beta)/\phi_\beta. \quad \text{(A1)}$$

Similarly

$$(\varepsilon_t - \varepsilon_\beta) = (\varepsilon_\alpha - \varepsilon_t)(1 - \phi_\beta)/\phi_\beta. \quad \text{(A2)}$$

Dividing equation (A1) by (A2) yields equation (9).

Derivation of the strain equation (15)

The strain ε in any direction θ given with respect to the long axis of the strain ellipse may be found from

$$1/(1 + \varepsilon)^2 = [\cos^2\theta/(1 + \varepsilon_1)^2] + [\sin^2\theta/(1 + \varepsilon_3)^2] \quad \text{(A3)}$$

(Ramsay 1967, pp. 65–66). For constant volume axisymmetric deformation

$$1 = (1 + \varepsilon_1)^2(1 + \varepsilon_3) \quad \text{(A4)}$$

and by definition

$$R = (1 + \varepsilon_1)/(1 + \varepsilon_3). \quad \text{(A5)}$$

Combining equations (A4) and (A5)

$$(1 + \varepsilon_1) = R^{1/3} \text{ and } (1 + \varepsilon_3) = [R(1 + \varepsilon_1)]^{-1/2}$$

which on substituting into (A3) and rearranging yields equation (15).

Derivation of the contiguity equation (28)

From equation (26)

$$(1 - C_\beta) = P_{\alpha\beta}/(2P_{\beta\beta} + P_{\alpha\beta}). \quad \text{(A6)}$$

The mean lineal intercept length of β is

$$d_\beta = \phi_\beta/N_\beta, \quad \text{(A7)}$$

where N_β is the number of β-grains intersected per unit test line length (Underwood 1970, p.81). In a two-phase material

$$N_\beta = (2P_{\beta\beta} + P_{\alpha\beta})/2 \quad \text{(A8)}$$

(Underwood 1970, pp.8–9). Substituting equation (A8) into equation (A7) yields equation (29), which substituting into equation (A6) and rearranging, gives equation (28).